Spectral Resolution Requirements for Mapping Urban Areas

Martin Herold, *Student Member, IEEE*, Margaret E. Gardner, and Dar A. Roberts, *Member, IEEE*

***Abstract*—This study evaluated how spectral resolution of high-spatial resolution optical remote sensing data influences detailed mapping of urban land cover. A comprehensive regional spectral library and low altitude data from the Airborne Visible/Infrared Imaging Spectrometer (AVIRIS) were used to characterize the spectral properties of urban land cover. The Bhattacharyya distance was applied as a measure of spectral separability to determine a most suitable subset of 14 AVIRIS bands for urban mapping. We evaluated the performance of this spectral setting versus common multispectral sensors such as Ikonos by assessing classification accuracy for 26 urban land cover classes. Significant limitations for current multispectral sensors were identified, where the location and broadband character of the spectral bands only marginally resolved the complex spectral characteristics of the urban environment, especially for built surface types. However, the AVIRIS classification accuracy did not exceed 66.6% for 22 urban cover types, primarily due to spectral similarities of specific urban materials and high within-class variability.**

***Index Terms*—Airborne Visible/Infrared Imaging Spectrometer (AVIRIS), Bhattacharyya distance, hyperspectral, Ikonos, Landsat, multispectral, spectral resolution, spectrometry, urban land cover.**

I. Introduction

URBAN environments represent one of the most challenging areas for remote sensing analysis due to high spatial and spectral diversity of surface materials. Typical urban surface types include a wide range of roofs, roads, sidewalks and parking lots of variable age, quality and composition. Further complicating the urban landscape are bare soil, vegetation, and other landscaping elements, creating a spectral diversity that far exceeds natural environments. This complexity, along with three-dimensional surface heterogeneity, creates a particularly challenging mapping environment for urban areas [1]–[4].

Urban mapping is further compounded by insufficient knowledge about the spectral properties of urban materials and spectral resolution requirements for separating them. With recent spectral and spatial sensor developments, there has been an increasing interest in urban spectral properties and mapping urban areas with remote sensing [5]. There are several questions yet to be answered: What spectral properties are characteristic for urban materials and how can they be discriminated from one another? What are the most suitable sensor spectral configurations for accurately mapping the urban environment? What are the capabilities and limitations of current high-resolution spaceborne sensors in mapping urban areas in terms of spectral resolution?

A few studies have focused on the spectral properties of urban materials. Ben-Dor *et al.* [5] acquired an urban spectral library from 400–1100 nm and discussed the importance of different spectral regions in mapping urban areas. The work of Heiden *et al.* [6], [8] and Hepner *et al.* [7] focused on the interpretation and analysis of urban spectral signatures. They found that spectra of urban built-up materials (e.g., roofs and roads) were best identified and separated by wavelength specific electronic and vibrational absorption features associated with mineral composition or other material properties.

In general, the spectral response from a land surface is strongly related to the sensor spatial resolution [9]. Several studies have reported problems in urban remote sensing due to limitations in spatial resolution [7], [10] or have presented a possible solution based on spectral mixture analysis [11]. Other studies suggest a spatial resolution of finer than 5 m for accurate representation of urban land cover objects such as residential structures or urban vegetation patches [12], [13]. Recently launched high spatial resolution spaceborne sensors such as the Ikonos camera (with 0.8-m panchromatic and 4-m multispectral resolution) and Quickbird (0.62-m panchromatic and 2.4-m multispectral resolution) meet this requirement and have the potential for more accurate and detailed mapping of urban land cover. The capabilities of these new satellite sensor systems are apparent in terms of their spatial and temporal resolution for urban area mapping. However, both spaceborne sensors are limited to four multispectral bands and may have specific spectral limitations in detailed urban area mapping.

The spectral resolution of a sensor can be characterized by the number of spectral bands, their bandwidths and locations along the spectrum. Spectral sensor resolution issues have been discussed since the early days of remote sensing, mainly due to the spectral limitations of sensors at that time. Recently, with continuous spectral coverage of hyperspectral sensors, interest has focused on band prioritization and/or selecting the most suitable wavelengths to map a specific environment [14]. Price [9], [15], for example, analyzed 45 AVIRIS scenes across a diversity of environments to determine the most important spectral bands for earth observation. He found that six AVIRIS bands described 99% of the spectral variability in all datasets, and that 20 bands described 99.9%. The band with the most spectral weight (at

Manuscript received September 13, 2002; revised April 7, 2003. This work was supported by the U.S. Department of Transportation, Research and Special Programs Administration, OTA under Contract DTRS-00-T-0002 (NCRST-Infrastructure).

M. Herold is with the Remote Sensing Research Unit, Department of Geography, University of California, Santa Barbara, CA 93106 USA (e-mail: martin@geog.ucsb.edu).

M. E. Gardner and D. A. Roberts are with the Department of Geography, University of California, Santa Barbara, CA 93106 USA (e-mail: meg@geog.ucsb.edu; dar@geog.ucsb.edu).

Digital Object Identifier 10.1109/TGRS.2003.815238

$\sim$ 1000 nm) is not currently available on an earth observation system, except for the experimental Hyperion sensor. However, the areas he investigated predominantly consisted of natural and quasi-natural nonurban landscapes. Price [15] attributed some of the variance undescribed by his optimal bands to urban or man-made features (e.g., roofs) and suggested that more or different bands would be required to spectrally assess these surface types. Initial studies have confirmed that hyperspectral data provide extensive spectral information that can discriminate urban materials on a very detailed level [5], [10], [16].

Large data volume and high correlation among spectral bands have been considered general problems in the analysis of hyperspectral data. Most image classification techniques require a reduction of spectral dimensions to a prioritized set of spectral bands that are sufficient for the application [14], [15], [17]. Different methods have been used for optimal band selection including principal component analysis (PCA), class separability measures and band correlation measures [9], [17]. Recently, the Bhattacharyya distance (B-distance) was proposed as a useful measure of separability [17], [18]. The B-distance is defined as [19]

$$B = \frac{1}{8}\left[\mu_1 - \mu_2\right]^T \left[\frac{\Sigma_1 + \Sigma_2}{2}\right]^{-1} \left[\mu_1 - \mu_2\right] + \frac{1}{2}\mathrm{Ln}\frac{\left|\frac{1}{2}\left[\Sigma_1 + \Sigma_2\right]\right|}{\sqrt{\left|\Sigma_1\right|\left|\Sigma_2\right|}}$$

where μ_i and Σ_i are the mean vector and the covariance matrix of class i, respectively. The B-distance is a sum where part one represents the mean difference component and part two the covariance difference component. Advantages of the B-distance include its close relationship to the probability of accurate classification [19] and its unlimited dynamic range is suitable for high-dimensional datasets. A general problem results from having no defined thresholds in terms of class separability. However, this measure can be used to assess separability of land cover classes and to prioritize bands that contribute most to spectral discrimination among the land cover classes of interest [14].

This study aimed for a better understanding of urban surface properties, their spectral representation, and the abilities of hyperspectral and recent high-resolution spaceborne remote sensing systems to map urban areas. This investigation identified the most suitable spectral bands for mapping the urban environment using a regional spectral library of field spectra and a local high-resolution AVIRIS dataset. Optimal bands, determined using the B-distance, were used to map urban land cover from AVIRIS data at a detailed level including 26 classes. To evaluate capabilities and limitations of multispectral systems and to suggest spectral improvements, AVIRIS results were compared to classifications generated from Ikonos and Landsat Thematic Mapper (TM), synthesized from AVIRIS. This study focused on the spectral component of image analysis. Other, higher order analysis factors such as spatial (e.g., texture), temporal (multiseasonal) or geometric (e.g., multiangle) information were not considered within the methodological framework of this study.

II. Data and Methodology

A. Study Area and Land Cover Characteristics

This study focused on a specific region in the urban area of Santa Barbara/Goleta, CA. This area is located 170 km northwest of Los Angeles in the foothills of the California Coast Ranges. The study area is characterized by a mixture of urban land cover types and surface materials including various categories of roof and road types of different age and condition.

A 4×2.5 km image subset of low topography was chosen for the specific analysis. The area was selected based on data availability and the representation of different man-made and quasi-natural land cover types. The western section is characterized by quasi-natural landscapes including agriculture, grasslands, shrublands, riparian areas and a lake. The central part of the image consists of single-family housing in a high-density residential area with different roof and road types, commercial and educational areas, and industrial land use in the southern central area. The eastern part is dominated by residential areas, including some multifamily housing complexes, as well as an area of downtown Goleta that represents an additional mix of urban materials. Development in the area occurred over several decades and therefore includes the many urban materials that have evolved in that time frame. This factor also contributes to the great spectral complexity of the area because spectral characteristics of materials can change over time.

Various classification levels were considered in this study as shown in Table I. Levels I and II represent functional categories and the main land cover classes based on the Anderson classification system [20]. Levels III and IV represent more detailed classifications of the urban environment. The thematic discrimination was based on the surface material (Level III) and color (Level IV). The class "red sport tartan" represents parts of sports facilities that usually appear next to tennis courts or running tracks in sports stadiums. Overall, 26 different land cover classes were considered in the analysis including four nonurban cover types (vegetation, bare soil, and water) and 22 urban categories (Table I).

B. Remote Sensing Data

This study used AVIRIS data acquired on June 9, 2000. The data were acquired at a spatial resolution of approximately 4 m, which is similar to current high spatial resolution spaceborne systems like Ikonos. They meet the generally proposed spatial resolution standard of less than 5 m for detailed urban area mapping [11], and the high spectral resolution allows for comparative analysis in urban land cover mapping. The AVIRIS sensor acquires 224 individual bands with a nominal bandwidth of 8–11 nm, covering a spectral range from 370–2510 nm [21].

The data were processed by the Jet Propulsion Laboratory (JPL) and the University of California, Santa Barbara (UCSB) for motion compensation and reduction of geometric distortions due to topography. The data were further georectified to match current digital databases of the study region. For this study, radiometrically corrected/georectified AVIRIS data were processed to apparent surface reflectance using modified Modtran radiative transfer code [22], [23], and further adjusted using a

TABLE I
LAND COVER CLASSIFICATION SCHEME FOR THE STUDY AREA

LEVEL 1	LEVEL 2	LEVEL 3	LEVEL 4
Built up	Buildings/roofs	Composite shingle roof	Brown/red shingle red
			Light Gray/white shingle
			Dark gray/black shingle
			Orange/tan shingle
		Gravel roof	Gray gravel
			Red gravel
		Metal roof	Brown metal
			Light gray metal
		Asphalt roof	Light gray asphalt
		Tile roof	Red tile
			Gray/brown tile
		Tar roof	
		Wood shingle roof	
	Transportation areas	Asphalt roads	Light asphalt (old)
			Dark asphalt (new)
		Concrete roads	
		Gravel roads	
		Parking lots	
		Railroad	
	Sport infrastructure	Tennis courts	
		Red sport tartan	
Vegetation	Green vegetation		
	Non-photosynthetic vegetation (NPV)		
Non-urban bare surfaces	Bare soil		
Water bodies	Natural/quasi-natural water bodies		
	Swimming Pools		

ground reflectance target [24]. Due to atmospheric contamination, the number of AVIRIS bands was reduced to 180, with the bands 1–7, 105–119, 152–169, 221–224 excluded from the analysis.

Multispectral bands of two common spaceborne systems, Ikonos and Landsat, were convolved from the AVIRIS data to investigate their abilities in urban mapping. This step used sensor specific spectral filter functions, available from the satellite providers, that were aggregated to AVIRIS wavelengths ($\sim$ 10-nm bandwidth). Fig. 1 shows the spectral response function for four multispectral Ikonos bands and six multispectral Landsat TM bands (bands 1–5 and 7). The functions are presented in values of normalized transmittance, indicating the contribution of each individual AVIRIS band to a specific multispectral sensor band. This information was used to synthesize Ikonos and Landsat TM data by summing the product between the normalized filter and any spectrum (pixel) from the AVIRIS scene, so all three datasets represent the exact same location, geometry, and spatial resolution.

C. Acquisition of ASD Urban Spectral Library

Field spectra were acquired with an Analytical Spectral Devices (ASD) Full Range (FR) spectrometer (Analytical Spectral Devices, Boulder, CO) on loan from JPL. The spectrometer samples a spectral range of 350–2500 nm. The instrument uses three detectors spanning the visible and near-infrared (VNIR) and shortwave infrared (SWIR1 and SWIR2). A fiber-optic cable transmits light from the aperture to the spectrometer. Both the bare fiber, with a field of view of 22°, and an 8° field of view foreoptic lens were used to acquire field spectra. More than 6000 spectra, including urban materials (e.g., various roof types and road materials) and nonurban surface types (e.g., green vegetation, nonphotosynthetic vegetation, and bare soil), were measured in the Santa Barbara urban area between May 23 and June 5, 2001. Spectra were acquired in sets of five for each field target. Four to six sets of spectra were bracketed by measurements of a Spectralon reflectance standard. Spectra were inspected for quality, and suspect observations were discarded. For this study, the spectral library was convolved to match the 224 AVIRIS bands based on the band center and the full width half maximum.

A small subset of spectra from the Santa Barbara spectral library is shown in Fig. 2. The graph represents the complex spectral characteristics of urban areas that makes urban remote sensing a challenging task. The urban cover types contain spectral signatures with large dynamic ranges, with a general increase in reflectance toward longer wavelengths. However, the shape of the reflectance increase varies for different urban targets. Small-scale spectral variations appear for several cover types representing the color (visible region) and absorption features due to material composition (SWIR region). Wood shingle roofs show ligno-cellulose absorption features in the SWIR typical of nonphotosynthetic vegetation surfaces. Some urban cover types, in particular specific road and roof types, have near constant, low reflectance, no significant broad absorption features and only minor differences in object brightness. Nonurban targets like vegetation and bare soil have well-established spectral properties with bare soil having the most similar reflectance to some urban cover types.

D. Database for Classification Accuracy Assessment

This study required a comprehensive ground truth database for classification training and accuracy assessment. This database was developed from ground mapping and low altitude photography, which was digitally compiled and processed. Critical issues for statistically robust accuracy assessment are the source and accuracy of reference information, the sampling size (i.e., how many sample points are necessary for each class), and the spatial sampling methods and units. These issues have been widely discussed in the related literature [25], [26]. In the complex urban environment, the number of individual classes is large, e.g., in this study 26, as are the intraclass spectral variances. At 4-m spatial resolution, most urban land cover objects such as buildings or roads cover small areas which are only represented by a few adjacent pixels. The edges or boundaries between individual land cover objects are fairly sharp, and it is usually easy to locate and assign a specific pixel to a land cover class.

Given these characteristics and the previous experiences described in the literature, a reference database for accuracy assessment was compiled based on the following assumptions.

- A large number of land cover classes and the expected low accuracy require a large number of samples per class, i.e., 100 individual samples.
- Ground mapping must focus on the acquisition and mapping of polygons representing individual land cover objects.
- Spatial random sampling is a statistically robust method but would not provide a comprehensive representation of all individual land cover classes. Accordingly, different

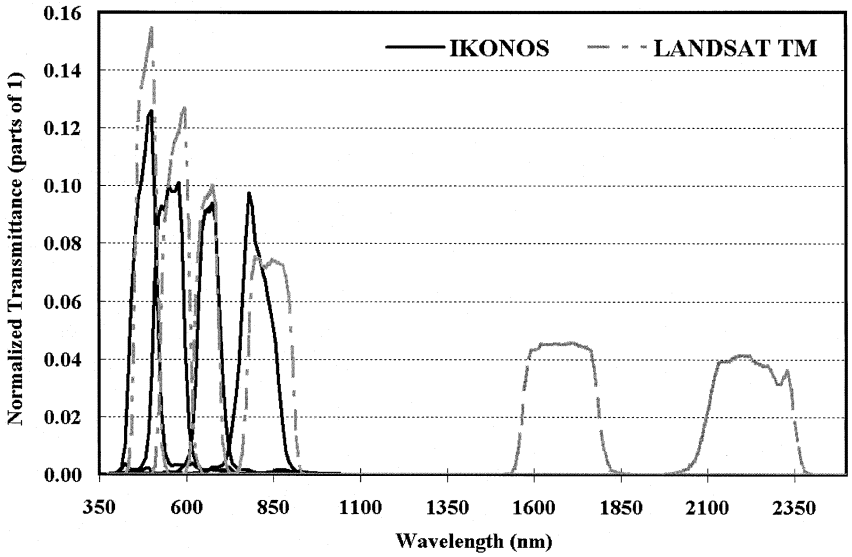

Fig. 1. Spectral response function for four multispectral Ikonos bands and six multispectral Landsat bands in normalized transmittance values convolved to 224 AVIRIS bands with 10-nm increments.

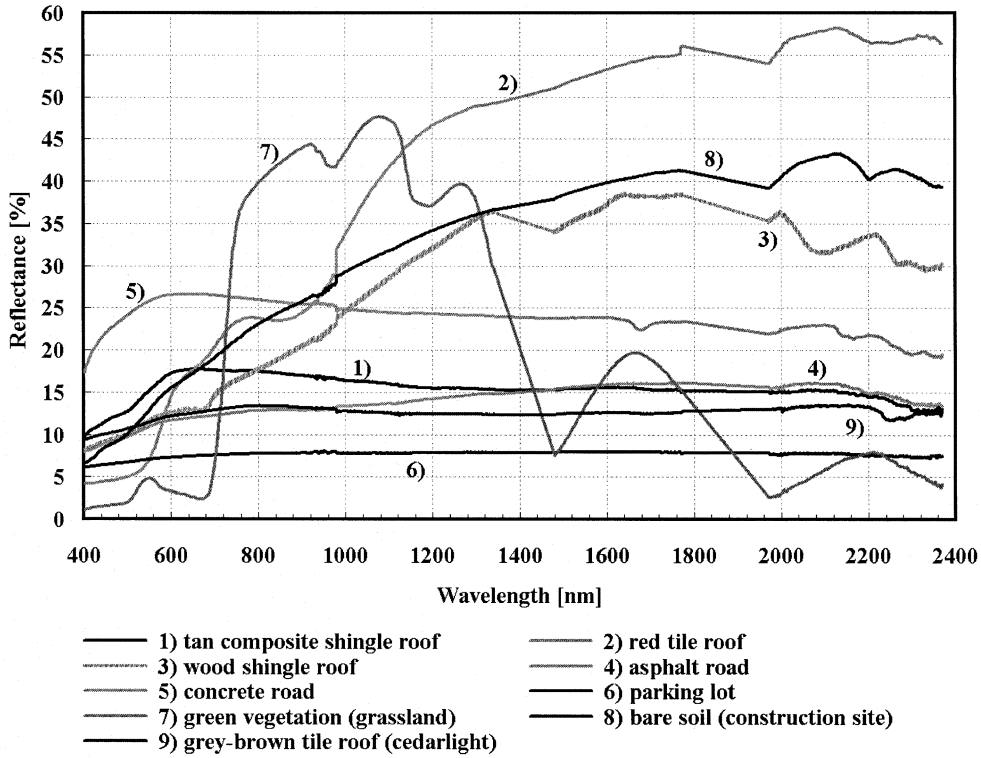

Fig. 2. Example spectra of typical urban land cover from the Santa Barbara spectral library (Note: the major water vapor absorption bands are interpolated).

spatial sampling methods should be used and explored for the ground mapping.

- The samples for accuracy assessment should be based on individual pixels rather than polygons to provide statistically independent points.

The ground mapping was based on three different spatial sampling schemes: spatial random sampling, and two systematic methods including neighborhood sampling and class-specific sampling. Spatial random sampling was applied by mapping roof types using a digital building footprint database. Analysis of the spatial random mapping results using 100 roofs showed that specific classes were underrepresented, especially for uncommon cover types. Furthermore, some sampled buildings were not accessible for mapping, e.g., on private property or buildings that were too small or no longer existed. Neighborhood sampling was applied to specific representative areas where every single roof and other surface types were mapped to better represent the variety of land cover classes in the study site. Neighborhood sampling provided the fastest mapping method used in this study but represents a systematic approach that requires *a priori* knowledge about the sampling area and the results depend on the location and size of the

mapping area. Finally, class-specific sampling was applied to derive additional sites that were not adequately sampled with the previous methods.

The three sampling schemes allowed a comprehensive database to be acquired that was digitally processed to support the image classification and data analysis (e.g., more than 350 individual roofs were mapped representing 10% of all roofs in the study area). For accuracy assessment, a spatial random sampling within the mapped polygons (stratified cluster sampling) was applied to derive 100 individual and statistically independent pixels for each land cover type to evaluate the classification performance. For one class, red sport tartan, only 73 pixels were available due to the small number of mapped sites.

E. Data Analysis and Image Classification

The methods used for data analysis included measures of spectral separability to determine the most suitable spectral bands for discriminating urban land cover types from the spectral library and the AVIRIS data, and for comparative image classification with different sensor spectral resolutions. All methodological analysis steps were applied using the public domain program "Multispec." This program was designed for the processing and analysis of hyperdimensional spectral datasets and contains procedures for the analysis of class separability and selection of most suitable spectral bands based on the B-distance and image classification [27].

The B-distance calculation considers the spectral information over the entire range (VIS-NIR-SWIR) and provides a separability score between each land cover class for a given set of spectral bands. This information can be used to identify the spectral bands that contribute the largest amount of spectral separation of these classes. The results can be aggregated to provide a set of most suitable bands based on best average and best minimum separability for the investigated categories. The B-distance calculation for the AVIRIS data were based on the 26 land cover classes presented in Table I. The most suitable bands from the spectral library were based on 108 different material types represented by over 4400 individual spectra.

The top score for best overall separability considers all possible band combinations and provides the maximum average B-distance score with the related set of most suitable wavelengths. The set of bands for best minimum separation is based on the best minimum B-distance value over all classes. The maximum number of bands available for each combination is limited by the lowest number of individual target spectra or training pixels. Given the limited number of individual spectra for specific cover types, there is a tradeoff between the exclusion of targets represented by a few number of spectral measurements and the maximum number of bands that can be considered in the analysis. In this study, the number of bands was limited to nine bands for best average and seven bands for best minimum separability for each dataset (spectral library and AVIRIS data).

To provide a more robust assessment of the most suitable bands the investigation considered the top 20 band combinations for best average and minimum separability. The resulting sets of bands were very similar for all top ranked combinations, hence usually only one or two bands differ between adjacently ranked sets of most suitable bands. The frequency of appearance of a band was considered a score for the importance of the band in land cover separation and can reach a maximum of 20 for either best average or best minimum separability.

Image classification was performed using a standard Maximum Likelihood classification technique implemented in "Multispec." The training areas were selected from the ground mapping database. The reference data for accuracy assessment were derived from the digital database (described in Section II-D) allowing for a statistically robust evaluation of the classification performance. The classification was performed for Ikonos and Landsat TM (convolved from AVIRIS) and from different sets of AVIRIS channels determined to be the most suitable bands for mapping urban land cover types. Accuracy assessment was used to evaluate the effects of spectral sensor resolution on mapping urban areas from high-resolution optical remote sensing data.

A more detailed analysis of the spectral limitations of Ikonos bands and possible improvements was performed by including particular optimal bands and recalculating the B-distance as a measure of separability. The investigations should represent the improvements in minimum separability for each of the 26 land cover classes by adding each AVIRIS band individually to the convolved bands of Ikonos and recalculating the B-distance. The results can be considered "spectra of improved separability" after subtracting the two B-distance values for every land cover class and each AVIRIS channel.

III. Most Suitable Spectral Bands in Separating Urban Land Cover Types

The most suitable wavelengths derived from B-distance separability analysis are shown in Fig. 3. The graph shows how often each spectral band is a member of the top 20 combinations of nine bands for best average separability and of seven bands for best minimum separability for each data source. In theory, a band can have a maximum frequency of 80 as it can appear in all of the top average and minimum channel combinations for the spectral library and the AVIRIS data. In Fig. 3, some bands have scores from 20 to 41 representing very important spectral bands in the spectral library, the AVIRIS data, or both. Some of the bands have a frequency of one. Most of these scores appear in a number of adjacent bands (e.g., in the visible region, at 1500 and 1700 nm) and represent an important "most suitable spectral region" without prioritization of a particular band. In the selection of the most suitable bands we considered the frequency score and whether the specific wavelength appears for both data sources (spectral library and AVIRIS) or for just one of them.

In general, suitable bands appeared in all parts of the spectrum. There are several bands in the visible region, a few in the NIR and several in the SWIR with a frequency of 20 or higher. The most important bands are marked with arrows in Fig. 3. The bands with bold arrows represent bands with a score of 20 or higher and are confirmed by the results from both the AVIRIS data and the spectral library. This confirmation is based on bands from each data source with a score of at least 20 spaced very close to each other or within an important spectral region

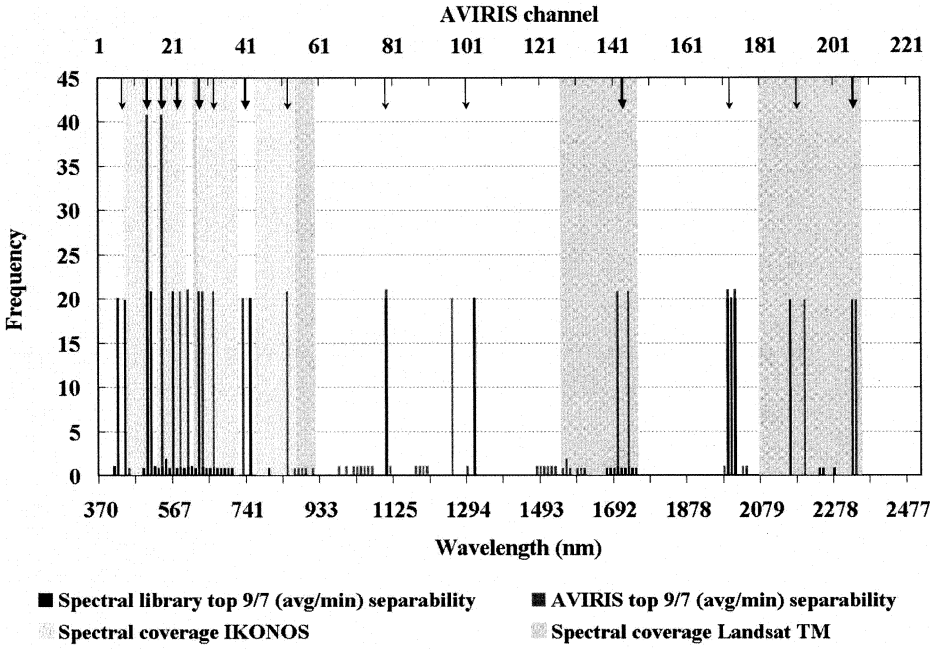

Fig. 3. Frequency of appearance of most suitable spectral bands for best average and minimum separability from the spectral library and AVIRIS data. The spectral coverage of Ikonos and Landsat TM satellite sensors are also shown.

(a consecutive number of score one bands). Seven bands are marked with bold arrows as very important. Four of them are in the visible region. These include two bands with a score of 20 at $\sim$ 498 nm (AVIRIS channel 14) and at $\sim$ 538 nm (AVIRIS channel 18) and two bands with a score of 21 from each data source at $\sim$ 580 nm (AVIRIS channel 22) and at $\sim$ 640 nm (AVIRIS channel 28). Further important bands are indicated in the NIR at $\sim$ 740 nm (AVIRIS channel 41) and the SWIR at $\sim$ 2330 nm (AVIRIS channel 207). They are emphasized by two adjacent bands from each source with a score of 20. Additional bands at $\sim$ 1710 nm (AVIRIS channel 143) are represented by two high score bands from AVIRIS data and a fair number of adjacent one-score bands from the spectral library.

Other suitable bands, marked with thin arrows, are not as strongly confirmed (e.g., are only represented in one data source). These bands are at $\sim$ 438 nm (AVIRIS channel 8), $\sim$ 675 nm (AVIRIS channel 32), $\sim$ 846 nm (AVIRIS channel 52), $\sim$ 1106 nm (AVIRIS channel 79), $\sim$ 1290 nm (AVIRIS channel 101), 2000 nm (AVIRIS channel 173), and $\sim$ 2180 nm (AVIRIS channel 191). The band near 2000 nm is strongly confirmed by the spectral library but is located within a CO_2 atmospheric absorption feature. This feature is slightly visible in the spectral signatures of the library and causes artifacts that do not represent material properties. However, this spectral region might still contribute important spectral contrast and was considered in the further analysis with careful treatment. Overall, the interpretations of Fig. 3 resulted in identifying 14 important individual spectral bands, seven of which can be considered particularly important, that were considered as the most suitable AVIRIS channels in the following investigations.

The distribution of the most suitable bands represents the spectral characteristics and variety of the land cover types found in this urban environment. There are several important bands in the visible region representing the diversity of color in urban land cover types. These bands are very close to each other emphasizing the important small-scale spectral variations between targets. There are four more bands in each of the VNIR and SWIR. These bands represent the spectral contrast in the region that relates to an increase in object brightness at longer wavelengths, characteristic of most urban targets. There are also specific absorption features due to material composition of different surface types that are represented in the most suitable bands, particularly in the SWIR region.

Fig. 3 also provides a comparison between the locations of the most suitable bands and the spectral coverage of the Ikonos camera and Landsat TM. The comparison shows that most of the suitable bands lie outside or near the boundaries of the spectral range of these sensors.

IV. Spectral Resolution in Urban Land Cover Classification

This section presents and discusses the classification results using the data analysis approach described in Section II. Based on the assumptions outlined in Section III we compared image classification results given different spectral sensor resolutions to explore current sensor systems capabilities and limitations and to define "optimal" sensor settings for detailed mapping of the urban environment. This section starts with the AVIRIS classification results using the most suitable set of spectral bands to show general capabilities and problems in detailed urban land cover mapping. Subsequently, we vary the spectral resolution used in image classification to elaborate on limitations in urban land cover mapping as a function of specific sensor characteristics.

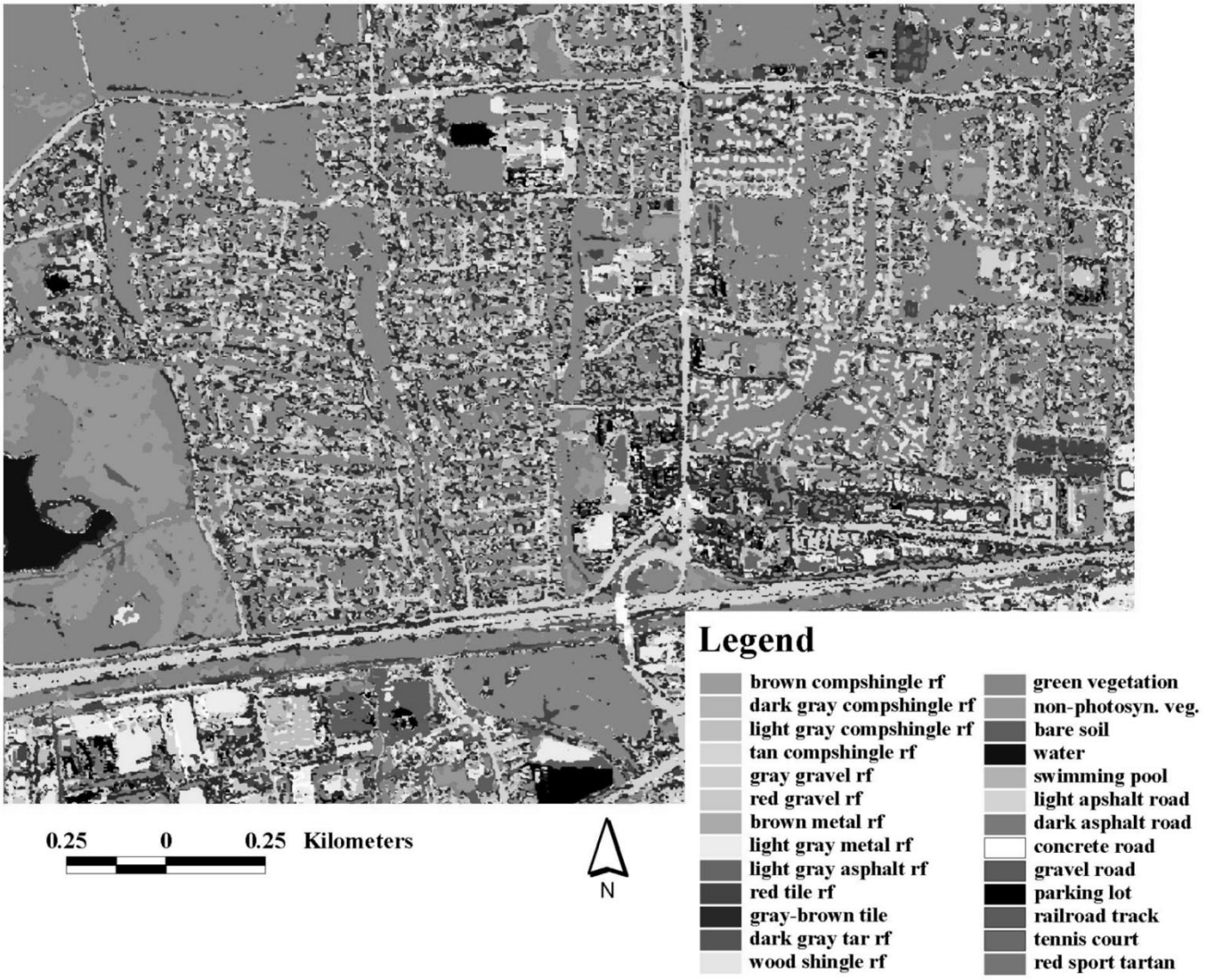

Fig. 4. AVIRIS classification result with 26 land cover classes.

A. AVIRIS Urban Land Cover Classification

The AVIRIS image classification utilized the set of 14 most suitable bands identified in Section III to derive 26 different land cover classes (Fig. 4). Most of the land cover classes appear as land cover objects comprised of several homogenously classified pixels. Vegetation patches, major roads and different urban land cover types are clearly identifiable in the classified image. Areas with a homogenous distribution of wood shingle roofs, dark gray composite shingle roofs and red tile roofs are accurately mapped in the upper right quadrant of the study area. The left part of Fig. 4 has a high-density residential area that shows very heterogeneous distribution of roof types. The industrial area in lower left is characterized by an increasing amount of bare soil cover.

These classification results show some inaccuracies as shown in the error matrix (Table II). The overall accuracy of the training sites was 98.6%, supporting the sophisticated training of the maximum likelihood classification. The overall accuracy using all reference pixels was 73.5% as mean increasing to 82.0% when weighted by class area. The difference is due to the high classification accuracy of large area classes such as green and nonphotosynthetic vegetation. The accuracy considering only the 22 urban classes (excluded are green vegetation, nonphotosynthetic vegetation, bare soil, and water; swimming pools are included) was determined to be 66.6%. Therefore, the nonurban classes can be mapped more accurately than the more complex urban classes. The Kappa of 72.5% represents the general precision that can be expected in mapping urban land cover on a very detailed level.

Some classes have particularly low accuracies. In terms of producer's accuracy, or general classification performance, accuracy levels of 40% to 70% were found for specific roof types including all types of composite shingle roofs, metal, asphalt, and red gravel roofs, and dark asphalt roads and parking lots. Low user's accuracies were also found for gray composite shingle, light gray metal, red tile, and gray-brown tile roofs and light asphalt roads. These classes were overmapped. Composite shingle roofs were most confused with composite shingle roofs of a different color, gray-brown tile roofs, and asphalt roads,

TABLE II
ERROR MATRIX OF THE AVIRIS URBAN LAND COVER CLASSIFICATION USING 14 MOST SUITABLE BANDS

	Producer's Accuracy (%)	Sample	1	2	3	4	5	6	7	8	9	10	11	12	13	14	15	16	17	18	19	20	21	22	23	24	25	26
1: br_comp_sh	**48**	100	48	5	3	7	--	--	--	--	--	1	28	--	--	--	--	--	--	--	--	--	--	--	--	--	--	--
2: dkgr_comp_sh	**50**	100	1	50	16	--	--	--	--	--	--	3	16	--	5	2	--	--	--	--	2	4	--	--	1	--	--	--
3: ltgr_comp_sh	**63**	100	--	15	63	--	9	--	--	6	--	1	4	--	--	1	--	--	--	--	1	--	--	--	--	--	--	--
4: tan_comp_sh	**52**	100	3	--	9	52	--	--	2	5	--	11	12	--	--	2	--	--	--	--	2	--	2	--	--	--	--	--
5: gr_gravel_rf	**95**	100	--	--	3	--	95	--	--	2	--	--	--	--	--	--	--	--	--	--	--	--	--	--	--	--	--	--
6: red_gravel_rf	**65**	100	--	--	--	--	--	65	--	2	--	15	14	--	--	4	--	--	--	--	--	--	--	--	--	--	--	--
7: brown_metal_rf	**62**	100	1	7	6	--	--	--	62	6	--	2	15	--	--	--	--	--	--	--	1	--	--	--	--	--	--	--
8: lt_gr_metal_rf	**69**	100	--	--	29	--	1	--	--	69	--	1	--	--	--	--	--	--	--	--	--	--	--	--	--	--	--	--
9: ltgr_asphalt_rf	**73**	100	--	--	18	--	3	--	--	5	73	--	--	1	--	--	--	--	--	--	--	--	--	--	--	--	--	--
10: red_tile_rf	**92**	100	--	--	--	--	--	--	--	1	--	92	6	--	1	--	--	--	--	--	--	--	--	--	--	--	--	--
11: grbr_tile_rf	**52**	100	2	8	11	1	--	--	4	5	--	13	52	--	1	--	--	--	--	--	1	1	--	--	1	--	--	--
12: dk_tar_rf	**43**	100	--	--	19	--	1	--	--	14	2	5	11	43	--	1	--	2	--	--	--	--	2	--	--	--	--	--
13: wood_sh_rf	**82**	100	--	--	1	--	--	--	--	2	--	8	4	--	82	3	--	--	--	--	--	--	--	--	--	--	--	--
14: green_veg	**95**	100	--	--	--	--	--	--	--	--	--	--	--	--	--	95	5	--	--	--	--	--	--	--	--	--	--	--
15: non_ph_veg	**100**	100	--	--	--	--	--	--	--	--	--	--	--	--	--	--	100	--	--	--	--	--	--	--	--	--	--	--
16: bare_soil	**81**	100	--	--	--	--	--	--	--	--	--	--	--	--	--	5	13	81	--	--	1	--	--	--	--	--	--	--
17: water	**98**	100	--	--	--	--	--	--	--	1	--	--	1	--	--	--	--	--	98	--	--	--	--	--	--	--	--	--
18: swim_pool	**96**	100	--	--	1	--	--	--	--	1	--	2	--	--	--	--	--	--	--	96	--	--	--	--	--	--	--	--
19: lt_asph_road	**89**	100	--	--	3	--	--	--	--	--	--	--	4	--	--	--	--	--	--	--	89	2	--	--	1	1	--	--
20: dk_asph_road	**55**	100	--	1	10	--	--	2	--	--	--	4	8	--	1	1	--	--	--	--	15	55	--	--	1	2	--	--
21: lt_concr_road	**71**	100	--	--	8	--	--	--	--	11	--	--	--	--	--	--	--	--	--	--	10	--	71	--	--	--	--	--
22: lt_gravel_road	**83**	100	--	--	--	--	--	--	--	15	--	--	--	--	--	--	--	1	--	--	1	--	--	83	--	--	--	--
23: parking_lot	**37**	100	1	1	5	--	--	--	--	2	--	3	5	--	--	4	--	25	--	--	12	3	--	--	37	2	--	--
24: railroad	**90**	100	--	--	3	--	--	--	--	--	--	1	1	--	--	--	--	--	--	--	5	--	--	--	--	90	--	--
25: gr_tennis_crt	**95**	100	--	--	--	--	--	--	--	--	--	4	--	--	--	--	--	--	--	--	--	--	--	--	--	--	95	1
26: red_sport_tar	**76.7**	73	--	--	--	--	--	--	--	--	--	17	--	--	--	--	--	--	--	--	--	--	--	--	--	--	--	56
	I. TOTAL	2573	56	87	208	60	109	67	68	147	75	183	181	44	90	118	118	109	98	96	140	65	75	83	41	95	95	57
	User's Accuracy (%)		**85.7**	**57.5**	**30.3**	**86.7**	**87.2**	**97**	**91.2**	**47**	**97.3**	**50**	**29**	**97.7**	**91**	**80.5**	**85**	**74**	**100**	**100**	**64**	**85**	**95**	**100**	**90**	**95**	**100**	**98**

OVERALL: Accuracy training areas= 98.6 % | Accuracy test sites: mean accuracy = 73.5 % / area weighted = 82.0 % / urban = 66.6 % / Kappa = 72.5%

which were commonly confused with light gray composite shingle roofs. A very poorly mapped category was gray-brown tile roof. This class was significantly overmapped due to confusion with several other roof types and asphalt roads, highlighting a typical problem in detailed urban mapping. For example, this class incorporates a fair number of gray/brown colored tile materials that vary with production company. Different roof conditions, age, and roof geometry further increase the within-class variability, contributing to the spectral complexity of the urban environment. The spectral signature of gray-brown tile roofs is similar to a fair number of other urban cover types, e.g., asphalt roads and composite shingle roofs (see Fig. 2). These classes do not clearly separate on the material scale. The interclass spectral contrast mainly results from object brightness. The gray-brown tile roofs have high within-class variability and are spectrally indistinct, resulting in low classification accuracy. This effect applies to several urban land cover classes with insufficient accuracy, e.g., composite shingle roofs, asphalt roads and light metal roofs. Even classes that have a very distinct spectral signature and are mapped with high producer's accuracy, such as red tile roofs (92%), can be significantly overmapped (user's accuracy) due to the large within-class variability.

B. Land Cover Classification With Varying Spectral Resolution

The land cover classification approach described above was repeated with the same training and test data sets for different settings of sensor spectral resolution. First, we evaluated the classification results for convolved Ikonos and Landsat TM versus AVIRIS (Table III). This table shows the improvement in mapping accuracy with increasing spectral resolution. The differences between Ikonos and AVIRIS accuracy ranges from

TABLE III
OVERALL LAND COVER CLASSIFICATION ACCURACIES FOR THREE DIFFERENT SPECTRAL SENSOR RESOLUTIONS

	MEAN	KAPPA	AREA WEIGHT	URBAN
Ikonos	61.8 %	60.2 %	66.6 %	37.7 %
Landsat	68.9 %	67.7 %	75.8 %	53.9 %
AVIRIS	73.5 %	72.5 %	82.0 %	66.6 %

$\sim 12\%$ for the mean overall accuracy and Kappa to $\sim 15\%$ for the area weighted accuracy and nearly 30% for the 22 urban classes. The improvements for built-up class mapping clearly confirm the limitations of Ikonos in detailed separation of urban land cover. Landsat TM data provided intermediate accuracies but showed the importance of having the SWIR bands (e.g., the improvements in classifying the urban cover types was more than 16% compared to Ikonos).

Fig. 5 compares producer's and user's accuracies obtained from each sensor for the individual land cover classes. The plots show that some classes have similar accuracies for all three sensors; hence there is no improvement by increasing the spectral resolution. Examples include green vegetation, water, and swimming pools. Nonurban classes, nonphotosynthetic vegetation and bare soil have a significantly higher accuracy for Ikonos and TM (producer's and user's) compared to urban classes using these sensors. AVIRIS provided only a slight improvement for these classes. Transportation areas were fairly similar in producer's accuracy except for light asphalt roads and railway tracks that were overmapped, especially in the AVIRIS data. In terms of user's accuracy, all transportation surfaces showed significant improvements as the spectral resolution of the sensor improved. Accordingly, a higher spectral resolution than Landsat TM should be preferred for detailed mapping of the transportation infrastructure.

Accuracy differences in roof type mapping were large with most roof classes showing significant improvements in producer's and user's accuracy with higher spectral resolution. Specific categories indicated more accurate classification between Ikonos and Landsat or between Landsat and AVIRIS, e.g., wood shingle roofs were already mapped accurately with Landsat and more spectral information would not be necessary. However, for most of the roof types the accuracy increased from Ikonos to TM and again from TM to AVIRIS. Examples included brown metal roofs, tar roofs, and gray brown tile roofs that showed significant classification improvements, and all types of composite shingle roofs. These roofs all have fairly low, near constant reflectance (see Fig. 2). The increasing number of bands better separated the cover types based on brightness and partly on small-scale absorption features that can be resolved in the AVIRIS data. However, Fig. 5 again shows some classes, in particular low reflectance targets that lack significant broad absorption features, with fairly low accuracy even in AVIRIS-based classification. Although a higher spectral resolution improves mapping accuracy, their classification accuracy is still insufficient, as discussed in Section IV-A. The difference in spectral resolution between the satellite sensors and the "optimal 14 band" AVIRIS configuration is related to two major issues. First, Ikonos and Landsat are broadband systems, while AVIRIS is not. Second, the sensors cover different spectral regions, e.g., the most suitable 14 bands are mostly located near the edge or outside the spectral coverage of these sensors (Fig. 3). To further elaborate on this issue and to test different configurations for an "urban mapping sensor" the land cover classification was performed for additional spectral resolution settings (Fig. 6). The graph shows the improvement in classification accuracy for three spectral sensor settings compared to the original Ikonos classification. These sensor configurations include the "optimal 5 VIS bands" representing the most suitable spectral bands in the visible and near-infrared that were derived in Section III at $\sim$ 498 nm (AVIRIS channel 14), $\sim$ 538 nm (AVIRIS channel 18), $\sim$ 580 nm (AVIRIS channel 22), $\sim$ 640 nm (AVIRIS channel 28), and $\sim$ 740 nm (AVIRIS channel 41). These bands generally cover a similar spectral region as Ikonos but represent narrower, more suitable bands for urban mapping. The second sensor configuration " Ikonos $+2$ optimal SWIR" uses the Ikonos bands plus two additional bands in the SWIR determined in Section III as most suitable (at $\sim$ 1710 nm—AVIRIS channel 143 and $\sim$ 2330 nm—AVIRIS channel 207). This configuration highlights the importance of including the most suitable SWIR bands for improved accuracy. The third setting "optimal 14" represents the 14 most suitable wavelengths used for the AVIRIS classification. This configuration provides the highest spectral resolution and the highest accuracy and has already been discussed in the previous sections.

The results in Fig. 6 show no improvements in sensor configuration for classes that are already well mapped by Ikonos like green vegetation, water and swimming pools. As expected, improvements are the highest for the "optimal 14" bands sensor configuration that correspond to the changes in accuracy presented in Fig. 5. By replacing the four broadband Ikonos channels with more suitable narrow bands ("Optimal 5 VIS bands"), there are significant improvements for nearly all roof types.

The enhancements are obvious in both producer's and user's accuracies for three types of composite shingle roofs, all tile, red gravel, tar, asphalt, and brown metal roofs. Either producer's or user's accuracy improves for tan composite shingle and gray metal roofs. The classification improves with the new configurations for bare soil and nonphotosynthetic vegetation. Additionally, transportation surfaces are more accurately mapped in terms of producer's accuracy for both types of asphalt roads and for all related classes in user's accuracy. The results clearly show the importance of having a system that can resolve small-scale spectral variations in the visible and near-infrared region due to color and the physical and chemical material properties of urban land cover classes.

Comparing the improvements of the "Optimal 5 VIS bands" and "Ikonos $+$ 2 optimal SWIR bands," the producer's accuracy is higher for nearly all classes from the "Ikonos $+$ 2 optimal SWIR bands." For the user's accuracy, the results are more mixed but the majority of classes show more improvement for the second sensor configuration (Ikonos $+$ 2 optimal SWIR bands). Examples include nonphotosynthetic vegetation, bare soil, all transportation cover types and several roof types. Wood shingle roofs show no improvements without the SWIR (see Fig. 2). The brown metal and red tile roof classes are clas-

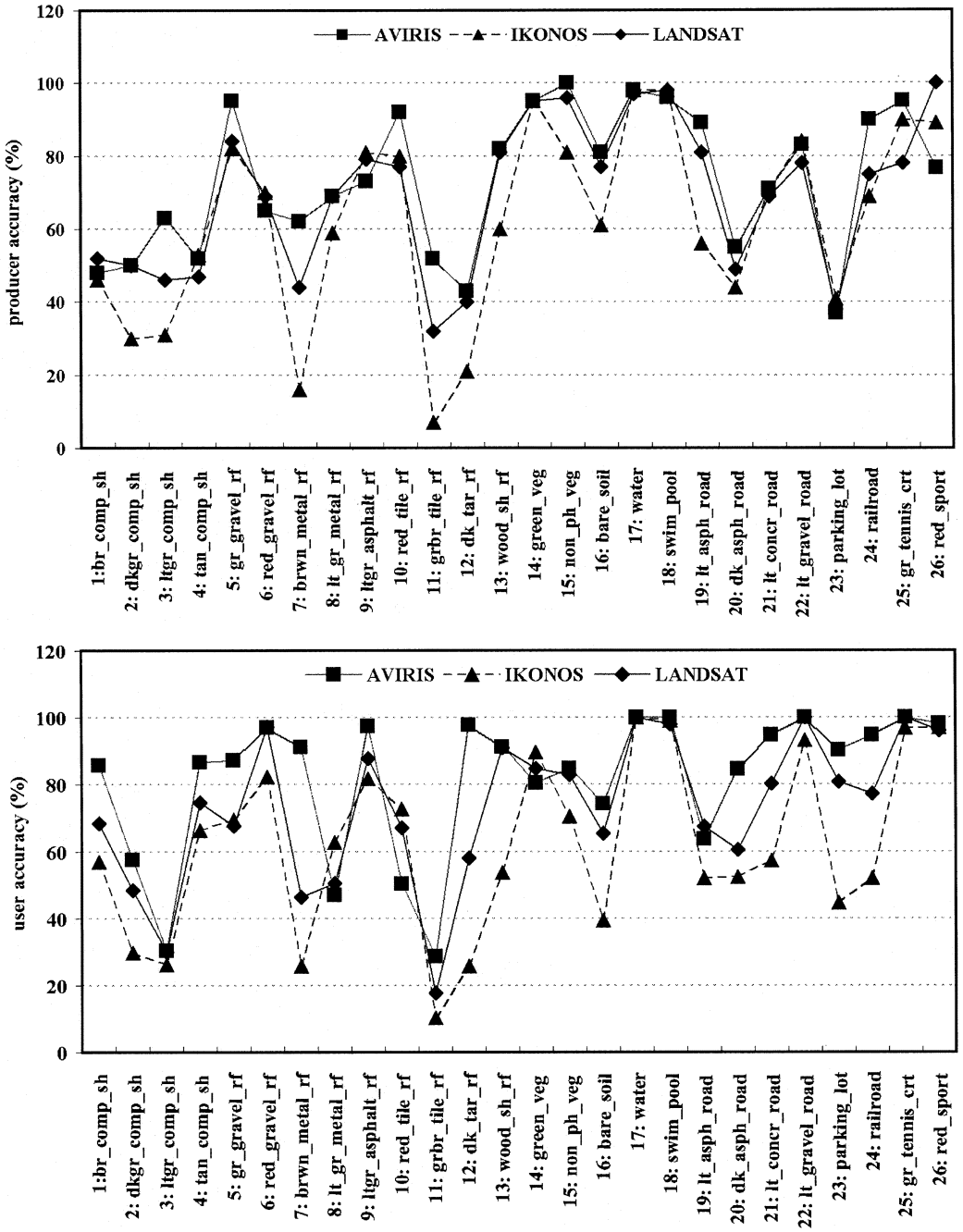

Fig. 5. Comparison of producer's (top) and user's accuracies (bottom) for land cover classification given the spectral sensor resolutions of Ikonos, Landsat TM, and AVIRIS (optimal 14 bands).

sified most accurately by the most suitable VIS/NIR bands indicating that a higher spectral resolution does not necessarily determine higher classification accuracy for all classes. However, considering the results presented here two suitable SWIR bands (in addition to the Ikonos channels) should be preferred to a narrowband VIS-NIR system with an optimized set of channels like the "Optimal 5 VIS bands" configuration.

This finding is supported by Fig. 7, which shows the spectra of improved separability measured by the B-distance (see Section II-E). The diagram shows that the best additional spectral separability of these cover types is found in the NIR and SWIR spectral regions not covered in Ikonos. Two main factors contribute to this observation. First, most urban land cover types show increased reflectance toward longer wavelengths that varies in terms of total reflectance change and the related spectral shape (e.g., convex or concave). The result is high spectral contrast in this region for the discrimination of those classes. Second, some of the urban targets have distinct absorption features in the SWIR region that are observed in the narrow AVIRIS bands, allowing a better separation and classification accuracy. Fig. 7 again shows the limitations resulting from the broadband character of the Ikonos channels that cannot resolve small-scale features in VIS/NIR. All classes shown in Fig. 7 indicate small improvement peaks in

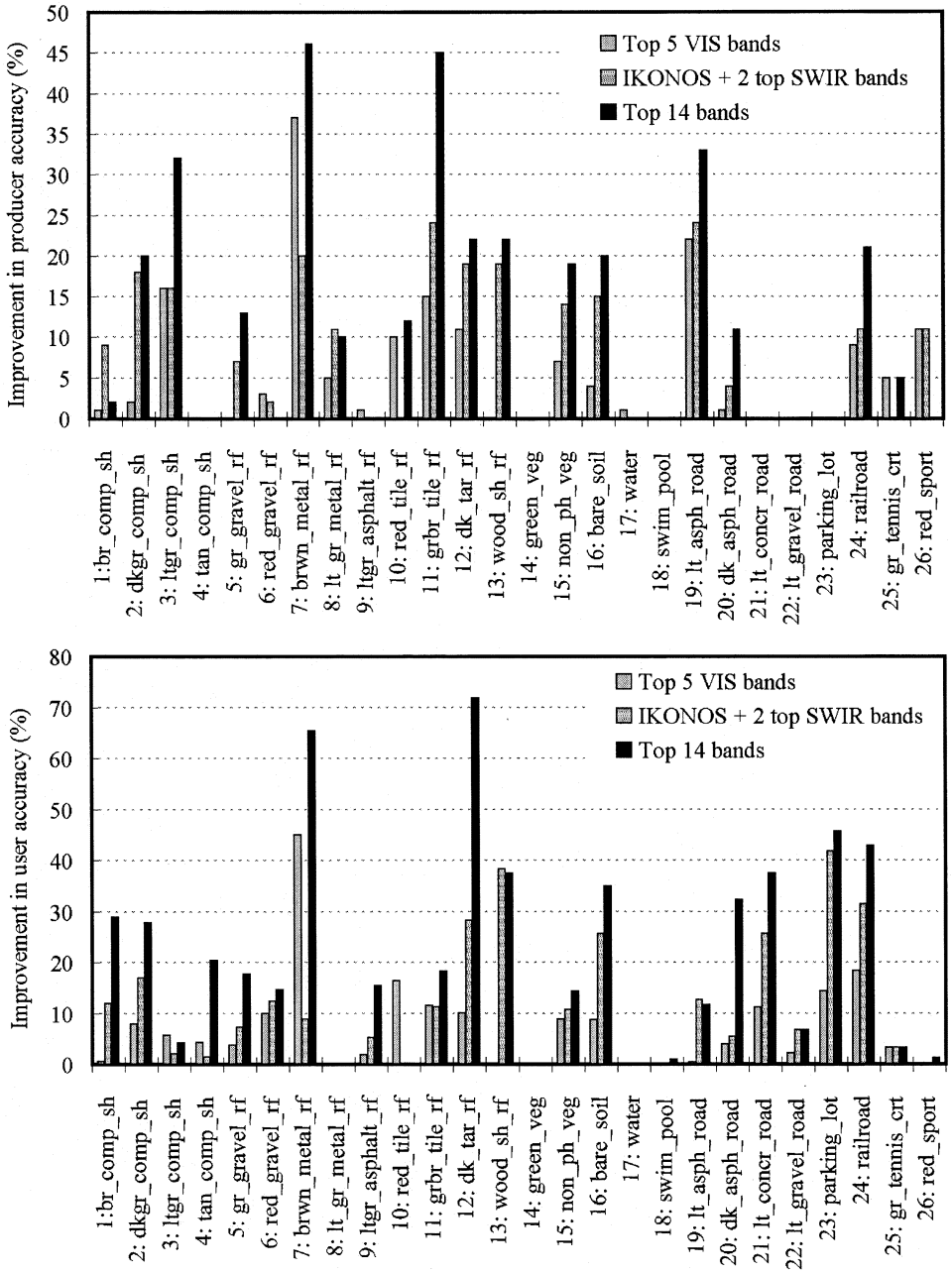

Fig. 6. Improvements in producer's (top) and user's accuracies (bottom) for three spectral sensor configurations compared to the mapping results from Ikonos.

the VIS/NIR and SWIR region that correspond to important small-scale spectral features. The most suitable AVIRIS bands represent these features well, suggesting that a well selected set of optimal narrow bands provides the most useful data source for mapping the urban environment.

V. Conclusion

This study investigated several issues concerning sensor spectral resolution in urban land cover mapping from high-spectral resolution remote sensing data. The analyses were based on a comprehensive regional spectral library, low altitude AVIRIS data in 4-m spatial resolution, and an extensive ground reference database for accuracy assessment and evaluation of the results.

A set of 14 optimal bands was derived for mapping the urban environment from the spectral library and the AVIRIS data. Most of these bands are located outside or near the edge of the spectral coverage of common satellite systems like Ikonos or Landsat TM. The expected spectral limitations of these systems were confirmed by the classification results. The difference between overall classification accuracy of urban classes was nearly 30% between Ikonos and AVIRIS and $\sim$ 13% between Landsat and AVIRIS with distinct differences for individual classes. Green vegetation, water and swimming pools were correctly mapped with Ikonos and there was no improvement with higher spectral resolution data. The classification accuracy of bare soil, nonphotosynthetic vegetation and wood shingle roofs significantly increased for the Landsat configuration with no significant enhancement in AVIRIS-based results. For

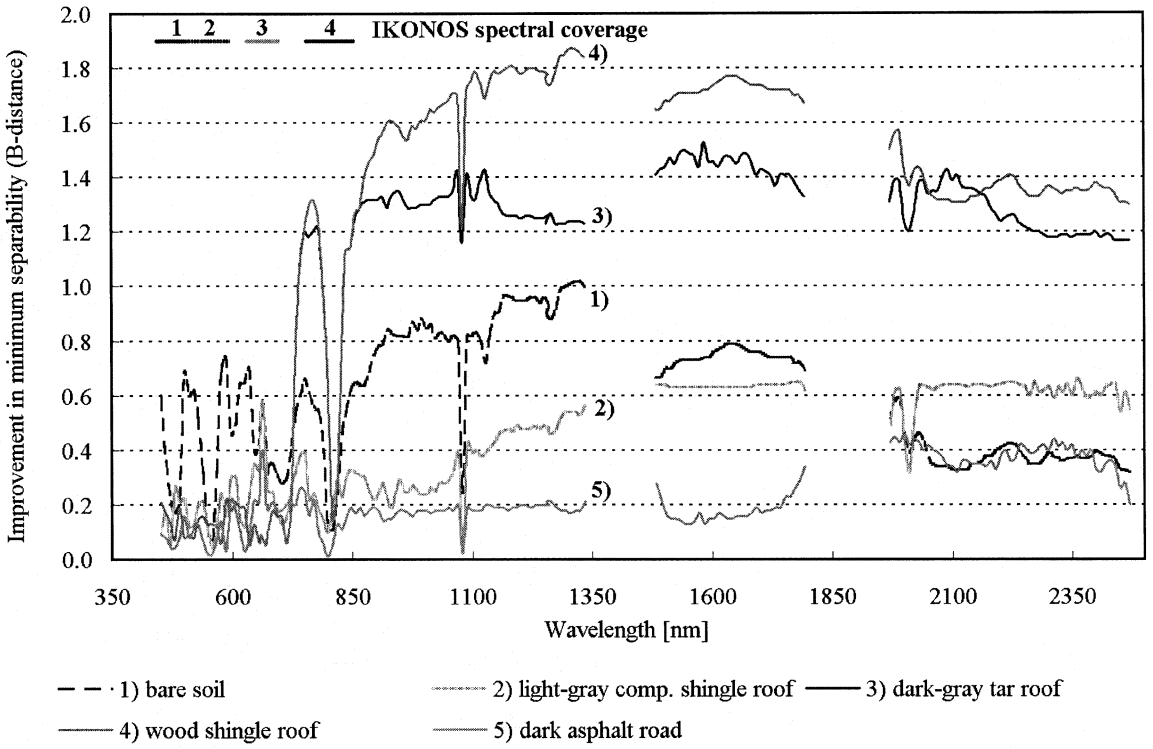

Fig. 7. Spectra of improved minimum class separability measured by the B-distance of five classes of Ikonos versus Ikonos bands plus every individual AVIRIS channel shown with the location of 14 most suitable bands in separation of urban land cover types (Note: Some of the artifacts in the presented spectra result from atmospheric interferences, e.g., $\sim$ 1080 and 2010 nm).

detailed mapping of different roof types and transportation infrastructure the AVIRIS sensor (represented by the 14 most suitable bands) clearly produced the best results. A more detailed evaluation of the Ikonos limitations showed improved mapping capability if the four broadband Ikonos channels were replaced by five narrow bands at more suitable wavelengths in the same spectral region. A classification considering the Ikonos bands plus two additional SWIR bands resulted in further improvement in map accuracy compared to maps generated using five narrow bands in the VIS/NIR region.

The importance of narrowband spectral information and the shortwave regions can be related to the spectral characteristics of urban land cover types. Most urban land cover types showed an increase in reflectance toward longer wavelengths that varied in terms of absolute reflectance change and the related spectral shape. Many urban targets have distinct small absorption features in all parts the spectrum. These features are important for land cover type separability and should be included to obtain higher classification accuracy. The unique spectral characteristics of the urban environment and the related required spectral resolutions can be provided by AVIRIS but not by common multispectral remote sensing systems.

The AVIRIS land cover classification of 26 different urban land cover classes illustrated general limitations in mapping the urban environment even using hyperspectral optical remote sensing data. Certain land cover types have very similar spectral characteristics. Some classes have a constant low reflectance over the whole spectral range with no or only minor distinct absorption features such as gray/brown tile, gray composite shingle and dark gray tar roofs, asphalt roads and parking lots. Considering the high spectral within-class variability due to roof geometry, condition, and age, their separability and classification accuracy was low, reaching only 66.6% for the 22 urban categories. However, this study produced a very detailed level of classification and applied only a pixel-based Maximum Likelihood classification algorithm on a purely spectral basis. Object-oriented or other classification techniques as well as spatial, textural or contextual information might provide a further significant improvement of map accuracy and help to overcome spectral similarities between specific classes. These approaches, when combined with spectral analysis presented in this study, provide a very interesting avenue for future research for more detailed and accurate urban mapping.

ACKNOWLEDGMENT

Georectified, radiometrically calibrated AVIRIS data were provided by the Jet Propulsion Laboratory, which also kindly supplied the ASD full-range instrument used in the field. The authors gratefully acknowledge the U.S. Department of Transportation for support of this research. The authors would like to thank P. Dennison, B. Hadley, and M. Wong for their support and valuable contributions to this project.

REFERENCES

[1] B. C. Forster, "Coefficient of variation as a measure of urban spatial attributes using spot HRV and Landsat TM data," *Int. J. Remote Sens.*, vol. 14, no. 12, pp. 2403–2409, 1993.

[2] G. J. Sadler, M. J. Barnsley, and S. L. Barr, "Information extraction from remotely sensed images for urban land analysis," in *Proc. 2nd Eur. Conf. Geographical Information Systems (EGIS'91)*, Brussels, Belgium, 1991, pp. 955–964.

[3] M. J. Barnsley, S. L. Barr, A. Hamid, P. A. L. Muller, G. J. Sadler, and J. W. Shepherd, "Analytical tools to monitor urban areas," in *Geographical Information Handling-Research and Applications*, P. M. Mather, Ed. Chichester, U.K.: Wiley, 1993, pp. 147–184.
[4] C. Small, "Scaling properties of urban reflectance spectra," in *Proc. AVIRIS Earth Science and Applications Workshop*, Palo Alto, CA, 2001, Available: [Online] http://popo.jpl.nasa.gov/docs/workshops/01_docs/2001Small_web.pdf.
[5] E. Ben-Dor, N. Levin, and H. Saaroni, "A spectral based recognition of the urban environment using the visible and near-infrared spectral region (0.4–1.1 m). A case study over Tel-Aviv," *Int. J. Remote Sens.*, vol. 22, no. 11, pp. 2193–2218, 2001.
[6] U. Heiden, S. Roessner, K. Segl, and H. Kaufmann, "Analysis of spectral signatures of urban surfaces for their area-wide identification using hyperspectral HyMap data," in *Proc. IEEE-ISPRS Joint Workshop on Remote Sensing and Data Fusion over Urban Areas*, Rome, Italy, 2001, pp. 173–177.
[7] G. F. Hepner, B. Houshmand, I. Kulikov, and N. Bryant, "Investigation of the integration of AVIRIS and IFSAR for urban analysis," *Photogramm. Eng. Remote Sens.*, vol. 64, no. 8, pp. 813–820, 1998.
[8] G. F. Hepner and J. Chen, "Investigation of imaging spectroscopy for discriminating urban land covers and surface materials," in *Proc. AVIRIS Earth Science and Applications Workshop*, Palo Alto, CA, 2002, Available: [Online] http://popo.jpl.nasa.gov/docs/workshops/01_docs/2001Chen_web.pdf.
[9] J. C. Price, "Spectral band selection for visible-near infrared remote sensing: Spectral-spatial resolution tradeoffs," *IEEE Trans. Geosci. Remote Sensing*, vol. 35, pp. 1277–1285, Sept. 1997.
[10] S. Roessner, K. Segl, U. Heiden, and H. Kaufmann, "Automated differentiation of urban surfaces based on airborne hyperspectral imagery," *IEEE Trans. Geosci. Remote Sensing*, vol. 39, pp. 1525–1532, July 2001.
[11] M. K. Ridd, "Exploring a VIS (vegetation-impervious-surface-soil) model for urban ecosystem analysis through remote sensing: Comparative anatomy for cities," *Int. J. Remote Sens.*, vol. 16, no. 12, pp. 2165–2185, 1995.
[12] C. E. Woodcock and A. H. Strahler, "The factor scale in remote sensing," *Remote Sens. Environ.*, no. 21, pp. 311–332, 1987.
[13] R. Welch, "Spatial resolution requirements for urban studies," *Int. J. Remote Sens.*, vol. 3, no. 2, pp. 139–146, 1982.
[14] C. I. Chang, Q. Du, T. Sun, and M. L. G. Althouse, "A joint band prioritization and band decorrelation approach to band selection for hyperspectral image classification," *IEEE Trans. Geosci. Remote Sensing*, vol. 37, pp. 2631–2641, Nov. 1999.
[15] J. C. Price, "An approach for analysis of reflectance spectra," *Remote Sens. Environ.*, vol. 64, pp. 316–330, 1998.
[16] P. Aplin, P. M. Atkinson, and P. J. Curran, "Fine spatial resolution simulated satellite sensor imagery for land cover mapping in the United Kingdom," *Remote Sens. Environ.*, vol. 68, no. 3, pp. 206–216, 1999.
[17] L. Jimenez and D. A. Landgrebe, "Hyperspectral data analysis and supervised feature reduction via projection pursuit," *IEEE Trans. Geosci. Remote Sensing*, vol. 37, pp. 2653–2667, Nov. 1999.
[18] C. Lee and D. A. Landgrebe, "Analyzing high dimensional multispectral data," *IEEE Trans. Geosci. Remote Sensing*, vol. 31, pp. 792–800, July 1993.
[19] D. A. Landgrebe, "Information extraction principles and methods for multispectral and hyperspectral image data," in *Information Processing for Remote Sensing*, C. H. Chen, Ed. River Edge, NJ: World Scientific, 2000, ch. 1.
[20] J. R. Anderson, E. E. Hardy, J. T. Roach, and R. E. Witmer, "A land use and land cover classification scheme for use with remote sensor data,", Reston, VA, U.S. Geological Survey Professional Paper 964, 1976.
[21] R. O. Green *et al.*, "Imaging spectroscopy and the airborne visible infrared imaging spectrometer (AVIRIS)," *Remote Sens. Environ.*, vol. 65, no. 3, pp. 227–248, 1998.
[22] R. O. Green, J. E. Conel, and D. A. Roberts, "Estimation of aerosol optical depth, pressure elevation, water vapor and calculation of apparent surface reflectance from radiance measured by th Airborne Vsible-Infrared Imaging Spectrometer (AVIRIS) using MODTRAN2," in *Proc. SPIE Imaging Spectrometry of the Terrestrial Environment*, 1993, pp. 2–5.
[23] D. A. Roberts, R. O. Green, and J. B. Adams, "Temporal and spatial patterns in vegetation and atmospheric properties from AVIRIS," *Remote Sens. Environ.*, vol. 62, no. 3, pp. 223–240, 1997.
[24] R. N. Clark, G. A. Swayze, K. B. Heidebrecht, A. F. H. Goetz, and R. O. Green, "Comparison of methods for calibrating AVIRIS data to ground reflectance," in *Proc. 4th Annu. Airborne Geosciences Workshop*, 1993, pp. 31–34.
[25] R. G. Cognalton and K. Green, *Assessing the Accuracy of Remotely Sensed Data: Principles and Practices.* Boca Raton, FL: Lewis Publishers, 1997, pp. 137–137.
[26] S. V. Stehman and R. L. Czaplewski, "Design and analysis of thematic map accuracy assessment: Fundamental principles," *Remote Sens. Environ.*, no. 64, pp. 331–344, 1998.
[27] D. A. Landgrebe and L. Biehl. (2002) An introduction to Multispec. [Online]. Available: Available: [Online] http://www.ece.purdue.edu/~biehl/MultiSpec/2001.

Martin Herold (S'98) was born in Leipzig, Germany in 1975. He received the the graduate degree (Diplom in Geography) from the Friedrich Schiller University of Jena, Germany and the Bauhaus University of Weimar, Weimar, Germany, in 2000. He is currently pursuing the Ph.D. degree at the University of California, Santa Barbara.

He has worked as a Researcher at the Department of Geography, Friedrich Schiller University of Jena, with a focus in multifrequency, polarimetric, and interferometric SAR data analysis for land surface parameter derivation and modeling. He joined the Remote Sensing Research Unit, University of California, Santa Barbara, in 2000, where his research interests are in remote sensing of urban areas and the analysis and modeling of urban growth and land use change processes.

Margaret E. Gardner was born in Knoxville, TN, in 1971. She received the B.S. degree in geography from James Madison University, Harrisonburg, VA, and the M.A. degree from the University of California, Santa Barbara (UCSB), in 1993.

She is currently a Researcher with UCSB, with a focus in hyperspectral remote sensing applications. She was a Remote Sensing Analyst and Project Manager for Pacific Meridian Resources, Emeryville, CA from 1998 to 1999.

Dar A. Roberts (M'94) was born in Torrance, CA, in 1960. He received the B.A. degree (double major in geology and environmental biology) from the University of California, Santa Barbara (UCSB), in 1981, the M.A. degree in applied earth sciences from Stanford University, Stanford, CA, in 1986, and the Ph.D. degree in geological sciences from the University of Washington, Seattle, in 1991.

He is currently an Associate Professor in the Department of Geography, UCSB, where he started in January 1994. His primary research interests are in remote sensing of vegetation, spectroscopy, hyperspectral remote sensing, land-cover mapping, change detection, sensor fusion, and algorithm development, primarily for spectral mixture analysis. He has worked extensively with airborne hyperspectral data since 1985, synthetic aperture radar since 1996, and most recently hyperspectral thermal imaging spectrometry data. He teaches an advanced graduate level course in microwave and optical remote sensing.

Dr. Roberts is a member of the Ecological Society of America, the Association of American Geographers, and the American Society of Photogrammetry.